

## Diphenylhexatrienes as Photoprotective Agents for Ultrasensitive Fluorescence Detection

Daniela Pfiffli,<sup>||,†</sup> Brigitte A. Bier,<sup>||,‡</sup> Christel M. Marian,<sup>\*,§</sup> Klaus Schaper,<sup>\*,‡</sup> and Claus A. M. Seidel<sup>\*,†</sup>

Chair for Molecular Physical Chemistry, Heinrich-Heine-Universität Düsseldorf, Universitätsstrasse 1, D-40225 Düsseldorf, Germany, Group for Organic Photochemistry, Division of Organic Chemistry, Institute for Organic Chemistry and Macromolecular Chemistry, Heinrich-Heine-Universität Düsseldorf, Universitätsstrasse 1, D-40225 Düsseldorf, Germany, and Institute of Theoretical and Computational Chemistry, Heinrich-Heine-Universität Düsseldorf, Universitätsstrasse 1, D-40225 Düsseldorf, Germany

Received: September 18, 2009; Revised Manuscript Received: February 1, 2010

Given the particular importance of dye photostability for single-molecule investigations, fluorescence fluctuation spectroscopy, and laser-scanning microscopy, refined strategies were explored for enhancing the fluorescence signal by selectively quenching the first excited triplet state of the laser dye Rhodamine 123 (**Rh123**). The strategy is to quench the  $T_1$  state by Dexter triplet energy transfer, while undesired quenching of the singlet state via Förster or Dexter singlet energy transfer and the generation of free radicals through electron transfer should be avoided. Diphenylhexatrienes (**DPHs**) were tested in ethanol for their beneficial effects as a novel class of photoprotective agents using fluorescence correlation spectroscopy. A library of **DPHs** with electron-donating (dimethylamino) and withdrawing substituents (e.g., trifluoromethyl) was synthesized to optimize the electronic properties. Quantum chemical calculations, optical spectroscopy, and cyclic voltammetry were used to determine the electronic properties. The computed  $T_1$  emission energy of **Rh123** and the  $T_1$  excitation energies of all **DPHs** allow for exergonic triplet energy transfer to the quencher. The parent compound quenches the  $T_1$  state of **Rh123** nearly diffusion controlled ( $4.9 \times 10^9 \text{ M}^{-1} \text{ s}^{-1}$ ). All electron-deficient **DPHs** significantly increase ( $3\times$ ) the fluorescence rate of **Rh123** by reducing the triplet state population and by avoiding the formation of other long-lived dark radical states. The quenching constants are reduced by more than a factor of 2, if substituents with increasing size or electronegativity are introduced. The beneficial effect of triplet quenching of substituted **DPHs** is governed by a delicate interplay of steric, electronic, and intermolecular Coulombic effects.

## 1. Introduction

Due to their high fluorescence quantum yields and high photostability, rhodamines<sup>1–3</sup> are important tools in confocal and superresolution microscopy,<sup>4,5</sup> single-molecule spectroscopy,<sup>6</sup> and fluorescence correlation spectroscopy (FCS).<sup>7</sup> Their beneficial properties are based on small singlet–triplet intersystem crossing (ISC) rates ( $k_{\text{ISC}} \approx 10^5\text{--}10^6 \text{ s}^{-1}$ ). Despite the low probability of this process compared to fluorescence emission ( $k_0 \approx 10^9\text{--}10^{10} \text{ s}^{-1}$ ), ISC to the long-lived first excited triplet state ( $^3F_1$ ) is a major limitation in single-molecule spectroscopy where high repetition rates of excitation and fluorescence are required. Under these conditions, the fluorescence dyes **F** will accumulate in the triplet state at higher irradiances and thus the signal saturates. Furthermore, the triplet state is involved in the photochemical destruction of the chromophore. Many attempts have been made to reduce the triplet lifetime in order to increase signal strength and photostability of free dyes<sup>8,9</sup> and bichromophores.<sup>10–13</sup> To this end, various cocktails and procedures have been used.<sup>8,14–20</sup>

Here, we suggest using quenchers **Q**, which selectively quench the triplet state, for this purpose. In principle, three different quenching mechanisms are feasible, quenching by dipole–dipole interaction (Förster mechanism),<sup>21–23</sup> quenching by electron exchange interaction (Dexter mechanism),<sup>24</sup> and quenching by redox processes.<sup>25–28</sup> Among these, the Förster mechanism can be excluded for triplet energy transfer, since its efficiency depends on the oscillator strength of the involved transitions.

In order to achieve efficient triplet excitation energy transfer (TEET) by the Dexter mechanism, certain conditions have to be fulfilled (Figure 1A). The quenching should be exergonic, and, at the same time, a significant overlap of the phosphorescence spectrum of the donor fluorophore ( $^3F_1 \rightarrow ^1F_0$ ) and the triplet-absorption spectrum of the quencher ( $^3Q_1 \leftarrow ^1Q_0$ ) is necessary.<sup>29,30</sup> Furthermore, to avoid singlet excitation energy transfer (SEET) by the Förster and Dexter mechanisms, the first excited singlet state of the quencher ( $^1Q_1$ ) should be located energetically above the fluorescing state ( $^1F_1$ ) of the fluorophore (Figure 1B). Additionally, undesired singlet quenching by oxidation (ox) or reduction (red) of the fluorophore has to be prevented (Figure 1C). The thermodynamic properties of the latter processes can be estimated using the Rehm–Weller equation<sup>25,26</sup> based on absorption spectra and ground-state redox properties:

\* To whom correspondence should be addressed. E-mail: cm@theochem.uni-duesseldorf.de; fax: +49 211 81 13466; tel: +49 211 81 13209 (C.M.M.). E-mail: schaper@klaus-schaper.de; fax: +49 211 81 14324; tel: +49 211 81 12571 (K.S.). E-mail: cseidel@gwdg.de; fax: +49 211 81 12803; tel: +49 211 81 15881 (C.A.M.S.).

<sup>†</sup> Chair for Molecular Physical Chemistry.

<sup>‡</sup> Institute for Organic Chemistry and Macromolecular Chemistry.

<sup>§</sup> Institute of Theoretical and Computational Chemistry.

<sup>||</sup> These authors contributed equally to this work.

$$\Delta G_{\text{ET}} = E_{\text{ox}} - E_{\text{red}} - \Delta E_{\text{n0}} - \Delta G^0(\epsilon) \quad (1)$$

where  $E_{\text{ox}}$  and  $E_{\text{red}}$  are the oxidation and reduction potentials of the electron donor and acceptor, respectively,  $\Delta E_{\text{n0}}$  is the singlet or triplet excitation energy.  $\Delta G^0(\epsilon)$  contains two correction terms based on the Born equation: (I) the interac-

tion energy of radical ions in a complex and (II) the effects of ion solvation. Because the investigated electron transfer reactions start with Rhodamine 123 (**Rh123**) in its cationic ground state and end up with a cationic quencher molecule, we neglect  $\Delta G^0(\epsilon)$  describing the solvation and the Coulomb interactions of the solvent-separated ion pair. Moreover, it is likely in protic solvents that proton-coupled reactions occur, which increase the feasibility of quenching.<sup>31</sup> The driving force for triplet quenching by redox processes is always smaller than the one for the singlet case, because the excitation energy  $\Delta E_{\text{n0}}$  is smaller for the triplet case (eq 1, Figure 1, and Tables 1 and 3). Thus selective triplet quenching by this mechanism is impossible.

Carotenoids with 11–13 conjugated double bonds are present in photosynthetic centers.<sup>32</sup> Besides functioning as antenna complexes, they are known to quench the  $T_1$  state of chlorophylls selectively, which otherwise would be an efficient sensitizer for singlet oxygen. However, for our purpose of quenching the triplet population of fluorescence dyes, these long-chained carotenoids are not suited because their optically bright  $1^1B_u^+$  state ( $S_2$  or  $S_3$ ) is low-lying. In addition, a dipole-forbidden transition to the  $S_1$  state ( $2^1A_g^- \leftarrow 1^1A_g^-$ ) takes place in the low-energy regime.<sup>33–35</sup> This dark  $2^1A_g^-$  state might be involved in undesired singlet quenching. Possible candidates with the desired quenching properties are carotenoids with shorter conjugation lengths. Here, aromatic pseudocarotenoids were investigated because these systems allow us to easily adjust the electronic properties by changing the substituents of the aromatic system.

For this purpose, a small library of diphenylhexatrienes (**DPHs**) with different electronic properties was synthesized (Figure 2A). Electron-donating and electron-withdrawing groups were introduced into the aromatic system in order to create compounds that were either (I) electron-rich [(*all-E*)-1,6-bis-[4-(dimethylamino)phenyl]hexa-1,3,5-triene (**Me<sub>2</sub>N-DPH**)],<sup>37,38</sup> (II) neutral [(*all-E*)-1,6-diphenylhexa-1,3,5-triene (**DPH**)],<sup>37,39,40</sup> or (*all-E*)-1,6-bis-(4-fluorophenyl)hexa-1,3,5-triene (**F-DPH**)],<sup>39,41–44</sup> or (III) electron deficient [(*all-E*)-1,6-bis-[4-(trifluoromethyl)phenyl]hexa-1,3,5-triene (**CF<sub>3</sub>-DPH**)],<sup>45</sup> (*all-E*)-1,6-bis-(4-cyanophenyl)-hexa-1,3,5-triene (**CN-DPH**)],<sup>37</sup> or (*all-E*)-1,6-bis-[3,5-bis(trifluoromethyl)phenyl]hexa-1,3,5-triene (**bis-CF<sub>3</sub>-DPH**)]. The electronic structures of these **DPHs** were determined using theoretical methods, the photophysical and electrochemical properties of the compounds were investigated, and their ability to selectively quench the triplet state was measured.

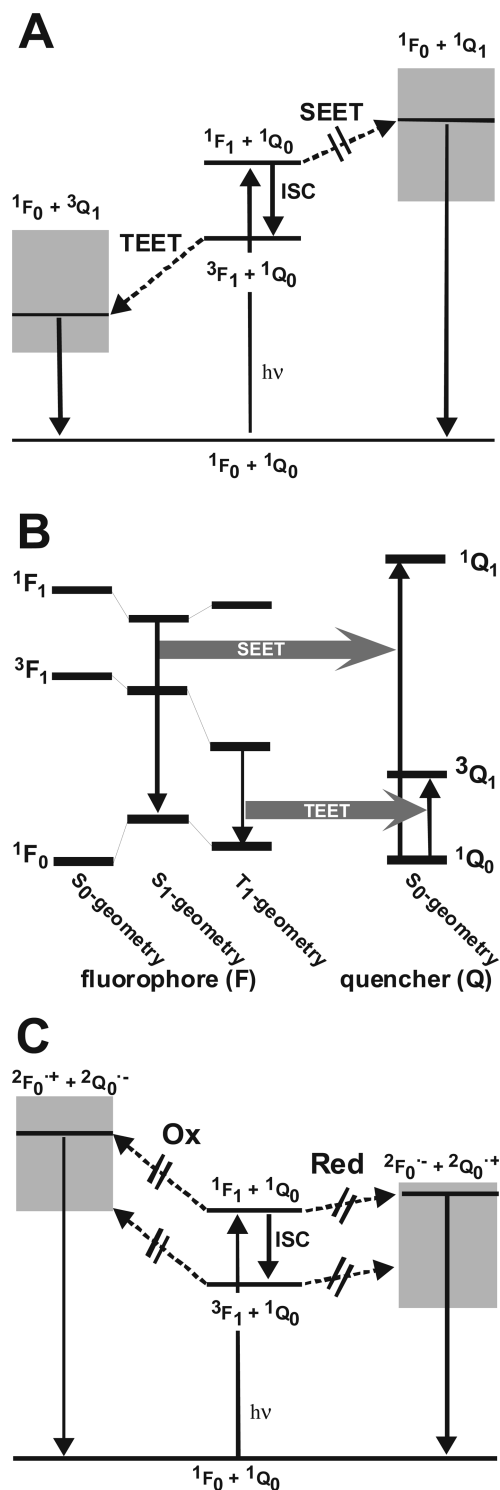


**Figure 1.** Overview of the energy of the states of fluorophore **F** and quencher **Q** involved in quenching processes. Depending on the nature of the quencher, these energies may vary (gray boxes). The desired values for these energies are marked by a black bar. (A) Energy balance for SEET and TEET. (B) Energies of individual states. (C) Possible electron transfer pathways.

## 2. Experimental Procedures and Computational Details

**2.1. Compounds.** The details of the synthesis and the analytical characterization of all products are given in the Supporting Information (SI, Section 1). In order to synthesize the desired compounds, we chose a strategy starting from substituted benzaldehydes and (*E*)-tetraethyl but-2-ene-1,4-diylidiphosphonate.<sup>40</sup> As a typical example, we describe the synthesis of **bis-CF<sub>3</sub>-DPH**. (*E*)-Tetraethyl but-2-ene-1,4-diylidiphosphonate (1.62 g, 4.93 mmol) was dissolved in 40 mL of dry tetrahydrofuran (THF). A 60% dispersion of sodium hydride in mineral oil (0.39 g, 9.8 mmol) was added with 10 mL of dry THF, and the mixture was stirred at room temperature for 30 min. To this mixture a solution of 2.73 g (11.3 mmol) of 3,5-bis(trifluoromethyl)benzaldehyde in 40 mL of dry THF was added dropwise over 5 min, and the mixture was stirred for another 30 min. A second dose of a 60% dispersion of sodium hydride in mineral oil (0.37 g, 9.3 mmol) was added with 10 mL of dry THF, and the mixture was stirred for 3 d at room temperature. Hydrolysis with 75 mL water causes the crude

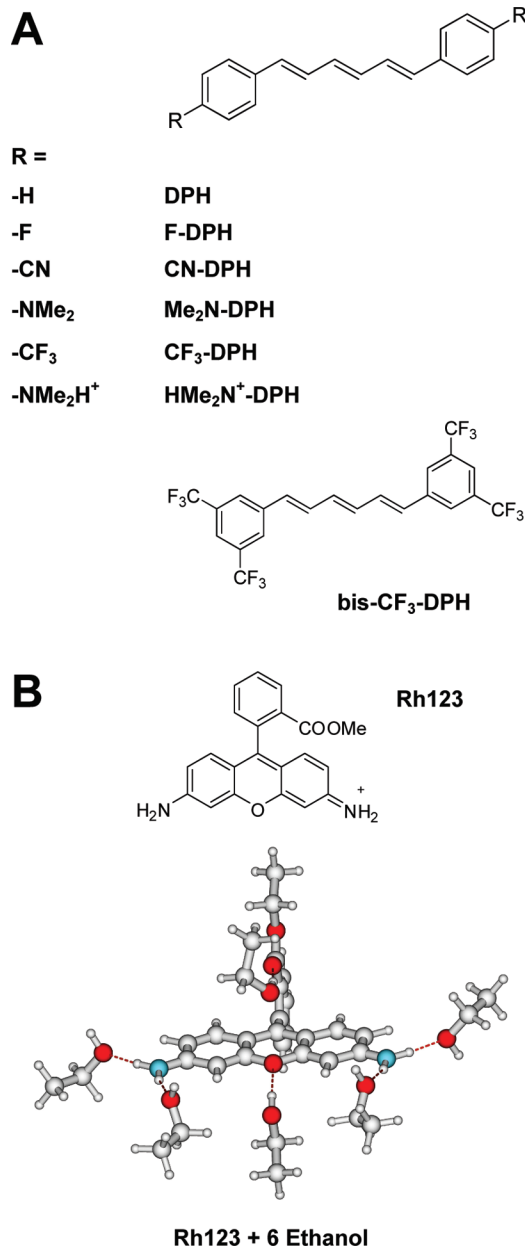


**Figure 2.** (A) Structures of **DPH** derivatives and (B) the **Rh123** structure<sup>36</sup> with six ethanol molecules.

product to precipitate, which was again solved in a little acetone and precipitated once more by adding hexane. Yield: 180 mg (7%). The absorption and fluorescence spectrum including a multi Gauss analysis are shown in Figure 3.

**Rh123** was purchased from Sigma Aldrich (R8004) and used as received. Solutions of **DPHs** in ethanol were prepared freshly and kept in the dark to avoid the photoinduced isomerization to a *cis*-isomere of the polyene.

**2.2. Calculations.** For the **DPHs** the valence triple- $\zeta$  basis set with (d) polarization function on all non-hydrogen atoms and (p) polarization function on hydrogen (TZVP)<sup>46</sup> was used. Test calculations on **Rh123** showed that excitation energies changed only marginally when the atomic orbital basis set was reduced to the less demanding split valence basis set with (d) polarization function on all non-hydrogen atoms (SV(P)).<sup>46</sup> For reasons of computer efficiency all calculations on **Rh123** were therefore carried out in the smaller SV(P) basis. The ground state geometries were determined using Kohn–Sham density functional theory (DFT)<sup>47</sup> with Becke’s three-parameter (B3LYP)

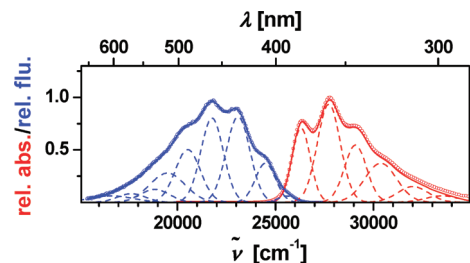


**Figure 3.** Absorption (red) and fluorescence (blue) spectra in THF (circles) and multi-Gauss analysis of the vibrational structure for **bis-CF<sub>3</sub>-DPH**. The resulting fits are given as solid lines; the individual Gauss curves are given as dashed lines.

exchange hybrid functional<sup>48</sup> and the correlation functional of Lee, Yang, and Parr.<sup>49</sup> Time-dependent density functional theory (TDDFT)<sup>50</sup> was employed for the <sup>1</sup>B<sub>u</sub> excited state geometry optimization of the **DPHs** and the S<sub>1</sub> state of **Rh123**. Unrestricted density functional theory (UDFT) was utilized for determining the minimum structures in the corresponding T<sub>1</sub> states. All geometry optimizations were performed with the TURBOMOLE 5.7 program package.<sup>51,52</sup> Solvent effects were taken into account only in case of the cationic dyes. To this end, explicit solvent molecules and a conductor-like screening model (COSMO) were employed.<sup>53</sup> The combined density functional theory/multireference configuration interaction (DFT/MRCI) method by Grimme and Waletzke<sup>54</sup> was used for single-point energy calculations at the obtained (TD)DFT equilibrium geometries. Recently, this method was shown to yield the correct order of excited states in  $\alpha,\omega$ -diphenylpolyenes<sup>55</sup> and  $\beta$ -carotenes.<sup>56</sup>

The technical parameters of the MRCI calculations were as follows. The 1s shells of all non-hydrogen atoms were kept frozen in the electron correlation treatments. The MRCI reference space was determined iteratively. The initial set was spanned by all single and double excitations from the five highest occupied molecular orbitals (HOMOs) to the five lowest unoccupied orbitals (LUMOs) of the ground state Kohn–Sham determinant. The final reference space consisted of all configurations that contributed with a squared coefficient of at least 0.003 to one of the six lowest roots in either the A<sub>g</sub> or B<sub>u</sub> irreducible representations (C<sub>2h</sub>-symmetric molecules), the six lowest roots in either the A<sub>g</sub> or A<sub>u</sub> irreducible representations (C<sub>i</sub>-symmetric molecules), or the 12 lowest roots (asymmetric molecules) in the first DFT/MRCI run.

The suitability of three different solvent models for describing the interaction between the **Rh123** chromophore and the solvent surrounding was tested at the ground-state geometry taking water as an exemplary solvent: (I) Microsolvation with six explicit water molecules that mimic the hydrogen bonds, (II) COSMO that accounts for the solvent polarity, and (III) a combination of I and II. It turned out that the red shifts brought about by COSMO alone (0.06 eV for S<sub>1</sub> and 0.08 eV for T<sub>1</sub>) are too small, whereas model I yields red shifts (0.15 eV for S<sub>1</sub> and 0.19 eV for T<sub>1</sub>) that are close to the solvent shifts (0.19 eV for S<sub>1</sub> and 0.23 eV for T<sub>1</sub>) obtained with our best model III. Moreover, model I has the advantage that it is applicable in excited state optimizations, too. We therefore chose model I for the calculation of the adiabatic singlet and triplet excitation energies of **Rh123** in ethanol solution (Figure 2B).

**2.3. Cyclic Voltammetry.** Redox potentials were determined by cyclic voltammetry (CV) in *N,N*-dimethylformamide (DMF). DMF (water-free, under nitrogen) was purchased from Aldrich. Tetra-*n*-butylammonium hexafluorophosphate (TBA PF<sub>6</sub>) was

used as received from Fluka and stored under argon. Dried argon was bubbled through the test solution for 15 min prior to and passed over the solution during the measurements. CV was performed with a potentiostat (Metrohm, AUTOLAB PGSTAT 20) and special software (GPES, Eco Chemie, version 4.9). The scan speed was 100 mV/s. A three electrode arrangement in a single cell was used for measurements: a thin Pt-sheet as the auxiliary electrode, a Ag/AgCl electrode as the reference electrode (Metrohm, 6.0726.100, 11040486), and a glassy carbon electrode (Metrohm, 6.1204.110) as the working electrode, which was polished with Al<sub>2</sub>O<sub>3</sub> powder in water after each measurement. The reference electrode was filled with 100 mM TBA PF<sub>6</sub> in acetonitrile. Ferrocene had an oxidation potential of 0.43 V against this reference electrode. As ferrocene has a half-wave potential of 0.69 V versus the normal hydrogen electrode (NHE), all reported potentials are cited against the NHE by adding 0.26 V to the measured ones. In electrochemical measurements, typical concentrations of the **DPHs** were 0.1–0.3 mM.

**2.4. Steady-State Spectroscopy.** All experiments were carried out at 25 °C in spectroscopic grade THF (nondegassed). Absorption spectra were recorded with a Varian-Cary 300 spectrometer. Fluorescence spectra were monitored with a Fluorolog-3 spectrometer (Jobin Yvon). To exclude polarization effects, the fluorescence of the probe was observed in a conventional 90° setup with a polarizer set to the magic angle (54.7°). For the measurements of the fluorescence quantum yields, the spectra were corrected for wavelength-dependent spectral sensitivity.

**2.5. Fluorescence Correlation Spectroscopy.** FCS was carried out with a confocal epi-illuminated microscope similar to that described before.<sup>15</sup> The fluorescent molecules are excited by a linearly polarized argon-ion-laser (Melles-Griot 35LAP431–230) at 496 nm in cw mode. The laser is focused into the sample by a water-immersion objective lens (UPLAPO 60 NA = 1.2, Olympus, Hamburg, Germany). In all measurements, the focal plane was 50 μm away from the coverslip. The fluorescence is collected by the same objective, separated from the excitation by a polychroic beam splitter (498 DCLP, AHF, Tübingen, Germany), and is detected by two avalanche photodiodes (Micro-Photon-Devices, PDM 50CT; Picoquant Berlin, Germany) in a beam splitting arrangement to eliminate dead time and afterpulsing artifacts. Fluorescence band-pass filters (HQ 533/46, AHF) block residual light and reduce Raman scattering from the solvent. A confocal pinhole of 80 μm diameter yields a characteristic diffusion time of 140 μs for **Rh123** in water. The signals of the two detectors are processed by a hardware correlator (ALV-5000, ALV-Laser, Langen, Germany). The measured correlation curves are fitted to different expressions for the FCS curves as stated, using a Levenberg–Marquardt nonlinear least-squares algorithm.

All measurements were performed in ethanol (Uvasol, Merck) at room temperature (20 ± 1 °C). To adjust the triplet lifetime, the solutions were purged with an O<sub>2</sub>–N<sub>2</sub> gas mixture with an oxygen content of approximately 0.1%.

### 3. Theory of Fluorescence Correlation Spectroscopy

FCS analyzes spontaneous fluorescence intensity fluctuations of fluorescent molecules excited in a focused beam with the correlation time  $t_c$ .<sup>57–59</sup> This fluctuation may be caused by a broad range of dynamic processes at the molecular level: changes in concentration of a fluorophore due to translation diffusion of the fluorescent molecules into and out of the sample volume element and changes in the excited singlet- or triplet-

state population. The time-dependent parts of the normalized correlation function can then be expressed as<sup>60</sup>

$$G(t_c) = 1 + \frac{1}{N_F} \left( \frac{1}{1 + t_c/t_d} \right) \left( \frac{1}{1 + (\omega_0/z_0)^2 t_c/t_d} \right)^{1/2} \times (1 - T_{eq} + T_{eq} \cdot e^{-t_c/t_T} - R_{eq} + R_{eq} \cdot e^{-t_c/t_R}) \quad (2)$$

$N_F$  is the mean number of fluorescent molecules within the sample volume element. The molecule detection function (MDF) is approximated by a three-dimensional Gauss distribution of the detected fluorescence with radial and axial  $1/e$  radii of  $\omega_0$  and  $z_0$ , respectively. The characteristic diffusion time  $t_d$  for the fluorescent molecules is related to the translational diffusion coefficient  $D$  by  $D = \omega_0^2/4t_d$ . Two bunching terms are possible: (I) the triplet bunching term is always needed, where  $T_{eq}$  is the mean fraction of fluorophores within the sample volume element being in their triplet states and  $t_T$  is the relaxation time of the triplet state, and (II) in case of radical formation a second bunching term is needed,<sup>8</sup> where  $R_{eq}$  is the mean fraction of fluorophore radicals and  $1/t_R$  is the radical relaxation rate given by the sum of rates for formation and decay of the radical. At low irradiances typical parameters of the MDF for **Rh123** in ethanol are as follows for the used O<sub>2</sub>–N<sub>2</sub> gas mixture:  $z_0/\omega_0 = 5.3$  and  $t_d = 240 \mu\text{s}$ . These parameters were left free in the fits of the data sets for a power series to compensate increasing optical saturation, which distorts the MDF.<sup>15,61</sup> As expected, both parameters increase significantly with rising irradiance and depend on the solvent as well as the degree of deoxygenation.

In the presence of micromolar concentrations of triplet quenchers  $[Q]$  and making the simplifying assumption of a uniform excitation profile within the detection volume, the expressions for  $T_{eq}$  and  $t_T$  are given by<sup>15,60,62</sup>

$$T_{eq} = \frac{k_{ISC}k_{01}}{(k_{ISC} + k_T')k_{01} + k_T'k_0} \quad (3)$$

$$t_T = \frac{k_{01} + k_0}{(k_{ISC} + k_T')k_{01} + k_T'k_0} \quad (4)$$

Considering a photophysical model with the three states  $S_0$ ,  $S_1$ , and  $T_1$ ,  $k_0$  is the deactivation rate of the first excited singlet state  $S_1$  to the ground singlet state  $S_0$ .  $k_{ISC}$  refers to the rate of intersystem crossing from  $S_1$  to the lowest triplet state  $T_1$  and  $k_T'$  is the effective rate of triplet state deactivation. The average excitation rate within the detection volume element depends on the average excitation intensity within the detection volume  $I_0/2$  and is given by  $k_{01} = \sigma_{01}(\lambda)\gamma I_0/2$ , where  $\sigma_{01}$  is the excitation cross section,  $\lambda$  is the excitation wavelength, and  $\gamma = \lambda/(hc)$  is the reciprocal photon energy, with  $h$  being Planck's constant and  $c$  being the velocity of light. The average intensity  $I_0/2$  is determined by  $I_0/2 = P/(\pi\omega_0^2)$ , where  $P$  is the laser intensity measured with a power meter.

The triplet quenchers with the bimolecular quenching constant  $k_{qT}$  influence the triplet deactivation by

$$k_T' = k_T + k_{qT}[Q] \quad (5)$$

where  $k_T$  is the effective rate of triplet state deactivation without quencher. The fluorescence count rate per molecule  $F_{cpm}$  is computed by normalizing the measured fluorescence signal  $F$

TABLE 1: Computed Energies of Various DPHs in the Gas Phase in Electron Volts

	vertical excitation at S <sub>0</sub> minimum <sup>a</sup>				adiabatic excitation <sup>b</sup>		vertical excitation at S <sub>1</sub> minimum <sup>c,d</sup>	
	S <sub>1</sub>	S <sub>2</sub>	T <sub>1</sub>	T <sub>2</sub>	S <sub>1</sub>	T <sub>1</sub>	S <sub>2</sub>	S <sub>1</sub>
	B <sub>u</sub> /A <sub>u</sub>	A <sub>g</sub>	B <sub>u</sub> /A <sub>u</sub>	A <sub>g</sub>	B <sub>u</sub> /A <sub>u</sub>	B <sub>u</sub> /A <sub>u</sub>	A <sub>g</sub>	B <sub>u</sub> /A <sub>u</sub>
<b>DPH</b>	3.34	3.51	1.81	2.85	3.10	1.39	2.79	2.94
<b>CF<sub>3</sub>-DPH</b>	3.28	3.46	1.77	2.80	3.06	1.37	2.75	2.90
<b>Me<sub>2</sub>N-DPH</b>	3.01	3.28	1.71	2.63	2.81	1.33	2.69	2.68
<b>F-DPH</b>	3.36	3.52	1.81	2.85	3.13	1.40	2.81	2.97
<b>CN-DPH</b>	3.05	3.26	1.69	2.64	2.84	1.31	2.60	2.69
<b>bis-CF<sub>3</sub>-DPH</b>	3.29	3.46	1.77	2.78	3.06	1.37	2.75	2.92
<b>HMe<sub>2</sub>N<sup>+</sup>-DPH</b>	3.18	3.43	1.75	2.79	2.97	1.36	2.80	2.84

<sup>a</sup> Comparable to the experimental absorption maximum (see Figure S5 and Table S1, SI). <sup>b</sup> Comparable to the 0–0 transition obtained from Gauss analysis of the experimental data (see Figure S5 and Table S1, SI). <sup>c</sup> Comparable to the experimental fluorescence maximum (see Figure S5 and Table S1, SI). <sup>d</sup> Except for **Me<sub>2</sub>N-DPH**, the order of the S<sub>1</sub> and S<sub>2</sub> states is reversed at this geometry.

TABLE 2: Experimental Energies of the Spectra of Various DPHs Measured in THF

	absorption				fluorescence	
	$\epsilon$ [M <sup>-1</sup> cm <sup>-1</sup> ] <sup>a</sup>	$f$ (L) <sup>b</sup>	$\Delta E_{\max}$ [eV] <sup>c</sup> ( $\lambda_{\max}$ [nm])	$E_{0,0}$ [eV] <sup>d</sup>	$\Delta E_{\max}$ [eV] <sup>c</sup> ( $\lambda_{\max}$ [nm])	$\Phi_F$ <sup>c</sup>
<b>DPH</b>	78 200	2.18	3.48(356)	3.30	2.73(455)	0.64
<b>CF<sub>3</sub>-DPH</b>	67 600	2.20	3.44(361)	3.26	2.86(434)	0.11
<b>Me<sub>2</sub>N-DPH</b>	69 300	2.49	3.06(408)	2.94	2.55(487)	0.33
<b>F-DPH</b>	59 200	2.11	3.50(354)	3.32	2.74(452)	0.58
<b>CN-DPH</b>	42 800	2.50	3.28(378)	3.09	2.74(453)	0.29
<b>bis-CF<sub>3</sub>-DPH</b>	62 300	2.08	3.44(360)	3.26	2.86(433)	0.08

<sup>a</sup> Extinction coefficients in ethanol. <sup>b</sup> Oscillator strengths obtained from DFT-MRCI calculations. <sup>c</sup> Maximum of the absorption/fluorescence spectra and fluorescence quantum yields in THF. The quantum yield of **DPH** was taken from literature and used as reference standard for the determination of the fluorescence quantum yields.<sup>64</sup> <sup>d</sup> Energy of the singlet state taken from the 0,0-transition from the multi-Gauss analysis (see Figure S5 and Table S1, SI).

to the total number of molecules  $N = N_F/(1 - R_{\text{eq}} - T_{\text{eq}})$  by taking the triplet fraction  $T_{\text{eq}}$  and the radical fraction  $R_{\text{eq}}$  into account:

$$F_{\text{cpm}} = \frac{F}{N_F}(1 - R_{\text{eq}} - T_{\text{eq}}) \quad (6)$$

## 4. Results and Discussion

**4.1. Energies and Spectra. Singlet States of DPHs.** Computed vertical excitation energies of all **DPHs** at their respective ground state geometries are collected in Table 1.

According to the calculations, the first excited singlet state is the  $1^1B_u$  state ( $1^1A_u$  in the lower symmetric **Me<sub>2</sub>N-DPH**) in the vertical absorption spectra of most compounds. It is mainly characterized by a single excitation from the HOMO to the LUMO. Geometry relaxation in the excited singlet state leads to an equalization of C–C bond lengths in the chain, similar to the situation in *all-E*-hexatriene.<sup>44</sup> For details, see Figure S4 of the SI.

The transition from the electronic ground state exhibits large oscillator strength  $f$  (2.1–2.5, see Table 2). The computed vertical excitation energy should be comparable to the Franck–Condon maximum of the corresponding experimental absorption spectrum.

The absorption and fluorescence spectra for all **DPHs** except **Me<sub>2</sub>N-DPH** are very similar (see Figures 3 and S5). Multi-Gaussian fits (full lines, Figures 3 and S5) were performed to characterize the spectral features of all spectra and the corresponding Stokes shifts. The progression of the lower vibronically excited states is about 1400 cm<sup>-1</sup> for all **DPHs** (see Table S1, SI). This value is typical for polyenes and averages two different vibrational modes at 1600 cm<sup>-1</sup> (C=C stretch) and 1200 cm<sup>-1</sup> (C–C stretch), which cannot be resolved in solution.<sup>63</sup> The

progression becomes smaller for higher excited states. The UV–vis absorption and fluorescence spectra show only a minute Stokes shift of approximately  $600 \pm 200$  cm<sup>-1</sup>. All experimental spectral properties are summarized in Table 2 (for a detailed discussion, see sections 2.2 and 2.3 of the SI).

The calculated vertical absorption energies are in good agreement with the maximum of the absorption spectrum. It should be noted, however, that the good agreement between theory and experiment is somewhat fortuitous. Benchmark calculations on linear polyenes and  $\alpha,\omega$ -diphenyl-polyenes<sup>55</sup> have shown that our theoretical approach systematically underestimates the electronic excitation energies of these compounds in the gas phase. This error is partially compensated by solvent effects, which are known to be strong for the  $1^1B_u \leftarrow 1^1A_g$  transition in **DPH**.<sup>65</sup>

Substitution in *para* or *meta* positions of the phenyl rings by CF<sub>3</sub> groups (**CF<sub>3</sub>-DPH**, **bis-CF<sub>3</sub>-DPH**) is found to have only minor effects on the electronic spectrum, but changes the redox potential significantly (see Table 3 below). In contrast, dimethylamination of **DPH** in *para* position (**Me<sub>2</sub>N-DPH**) or introduction of a cyano group (**CN-DPH**) in this position has a large influence on the spectral properties. Both types of substitution lead to an effective increase of the conjugation lengths and a red shift of the absorption maximum. The obtained data (Table 2, Figure S5 in the SI) show that the trends observed for the vertical and adiabatic absorption energies of the compounds are reproduced well by our theoretical approach. On the average, the calculated vertical absorption energies are too small by 0.1 to 0.15 eV, only for **CN-DPH** is the error 0.2 eV. For the adiabatic transitions, errors are slightly larger.

**Singlet States of Rh123.** Considering the fluorophore **Rh123** in vacuum, vertical excitation energies for absorption  $E_{S,\text{vac}}(1^1F_1 \leftarrow 1^1F_0) = 2.70$  eV and fluorescence  $E_{S,\text{vac}}(1^1F_1 \rightarrow 1^1F_0) = 2.60$  eV were computed. However, since rhodamines are highly

**TABLE 3: Measured Oxidation and Reduction Potentials and the Estimated Standard Free Energy of the Reductive Electron Transfer by Eq 1 between Quencher and the  $S_1$ ,  $T_1$  and Radical Cation State  $R^{+\cdot}$  of Rh123 in Ethanol<sup>a</sup>**

quencher	[V] vs NHE		$\Delta G_{ET}$ [eV] reduction of Rh123				$k_{qT}$ [ $10^9$ M <sup>-1</sup> s <sup>-1</sup> ]
	$E_{ox}^b$	$E_{red}^b$	$S_1$	$T_1$	$R^{+\cdot}$		
<b>Me<sub>2</sub>N-DPH</b>	0.57 <sup>#</sup>	-1.92	-1.23	-0.72	-0.64	$6 \pm 1^c$	
<b>F-DPH</b>	1.26	-1.73	-0.54	-0.03	0.05	$2.9 \pm 0.3$	
<b>DPH</b>	1.28	-1.71	-0.52	-0.01	0.07	$4.9 \pm 0.6$	
<b>CF<sub>3</sub>-DPH</b>	1.42	-1.50	-0.38	0.13	0.20	$2.5 \pm 0.2$	
<b>CN-DPH</b>	1.42	-1.29 <sup>#</sup>	-0.38	0.13	0.20	n.d.	
<b>bis-CF<sub>3</sub>-DPH</b>	1.52	-1.44	-0.28	0.23	0.30	$2.1 \pm 0.7$	

<sup>a</sup> All oxidative processes were estimated to be  $\Delta G_{ET} > 0$ . For the calculation of the redox potentials of Rh123,  $E_{ox} = 1.21$  V vs NHE and  $E_{red} = -0.61$  V vs NHE, and the energies of the  $S_1$  and the  $T_1$  state,  $E_S = 2.41$  eV and  $E_T = 1.90$  eV were used. The contribution of the Coulomb term is assumed to be negligible. The estimated errors for the measured potentials are  $<0.05$  V. The precision for the quenching rates corresponds to the statistical error of the linear fit for the slope (eq 5). The accuracy (systematic error) is mainly due to errors in the determination of the quencher concentration via UV/vis absorption spectroscopy using the extinction coefficients in Table 2 ( $<5\%$ ). <sup>b</sup> All peaks were irreversible unless they are indicated with a number sign (#). <sup>c</sup> Estimated quenching rate due to additional dark state; see section 4.3.

polar molecules, a distinct solvent effect is expected. Complexation by six explicit ethanol molecules (Figure 2B, solvation model I) results in a reduction of the energies to  $E_{S,solv}(^1F_1 \rightarrow ^1F_0) = 2.44$  eV (508 nm) and  $E_{S,solv}(^1F_1 \rightarrow ^1F_0) = 2.32$  eV (534 nm), respectively. These calculated transition energies of **Rh123** in ethanol agree nicely with the experimental energies for the maximum absorption and fluorescence,  $\Delta E_A = 2.43$  eV (511 nm) and  $\Delta E_F = 2.34$  eV (530 nm), respectively.

**Triplet States of DPHs.** In the **DPH** derivatives two triplet states  $T_1(B_u/A_u)$  and  $T_2(A_g)$  are found below  $S_1$  (see Table 1). As for  $S_1$ , the electronic structure of  $T_1$  is mainly characterized by a single excitation from the HOMO to the LUMO. However, unlike  $S_1$ , geometry relaxation in the first excited triplet state leads to an inversion of single and double bonds in the chain, as observed previously for *all-E*-hexatriene<sup>55</sup> (for details see SI Section 2.1 and Figure S4). Within the accuracy of our computational method, the vertical  $T_1$  excitation energy  $E_T(^3Q_1 \leftarrow ^1Q_0) = 1.76 \pm 0.05$  eV is the same for all **DPHs**. This applies also to the adiabatic energy  $E_T(^3Q_1 \rightarrow ^1Q_0) = 1.36 \pm 0.04$  eV. Experimental values for the triplet energies  $E_T$  of the parent compound **DPH** are available from energy transfer experiments in solution ( $E_{T,solv} = 1.47-1.54$  eV).<sup>66-68</sup> As the computed energies agree satisfactorily with experimental values, we assume that the accuracy of these triplet calculations is as good as the ones for absorption and fluorescence of the singlet states. It is noteworthy that the effect of substituents on the adiabatic excitation energy of the  $T_1$  state is much less pronounced than in the singlet case.

**Triplet State of Rh123.** The vertical triplet excitation energy  $E_T(^3F_1 \leftarrow ^1F_0)$  of **Rh123** at the  $S_0$ -geometry was computed to 2.14 eV in vacuum and to 1.86 eV in ethanol. Similar to the singlet case, the formation of hydrogen bonds causes a substantial red shift of the excitation wavelength. At the triplet minimum geometry, a vertical emission energy of 2.02 eV (vacuum) and 1.76 eV (ethanol) is obtained. The calculated adiabatic  $^3F_1$  emission energy in ethanol solution (solvation model I) amounts to 1.82 eV. No experimental values have been reported for the triplet energy of **Rh123**. However, experimental triplet data (maximum of the phosphorescence spectrum,  $\Delta E_P = 1.90$  eV (651 nm))<sup>69,70</sup> are available for the related derivative Rhodamine 110 (**Rh110**), where the carboxyphenyl residue is not esterified. We expect very similar molecular energies because the maxima of the absorption and fluorescence spectra of **Rh123** are only slightly red-shifted by 1 to 2 nm with respect to **Rh110** (maxima of singlet absorption,  $\Delta E_A = 2.43$  eV (510 nm); fluorescence,  $\Delta E_F = 2.35$  eV (528 nm)). Comparison of the experimental values for **Rh110** with our computed excitation energies for **Rh123** shows that

our DFT/MRCI results slightly underestimate the true excitation energies but are in the right ballpark, in line with general trends observed for this method.<sup>71</sup>

**Free Energies for Energy Transfer Reactions.** In order to avoid singlet quenching of a fluorophore by SEET (see Figure 1B), the condition  $E_S(F) < E_S(Q)$  must be fulfilled for the singlet energies. This condition is met even for the quencher **Me<sub>2</sub>N-DPH** with the most red-shifted absorption maximum, for which  $E_S(^1Q_1 \leftarrow ^1Q_0)$  was measured to be 3.01 eV, i.e. SEET of **Rh123** to any of these **DPHs** is endergonic. For our **DPHs**, the optically dark  $2^1A_g$  state, which constitutes the first excited singlet state in longer carotenes, is located slightly above the  $1^1B_u/1^1A_u$  state at the ground-state geometry.

The condition for efficient triplet quenching of **Rh123** by TEET (see Figure 1B),  $E_T(F) > E_T(Q)$ , is fulfilled by all **DPHs**, and the spectral overlap between donor and acceptor should be good.

**4.2. Redox Properties.** To judge whether photoinduced electron transfer reactions can be a relevant quenching pathway, the oxidation and reduction potentials,  $E_{ox}$  and  $E_{red}$ , of the **DPHs** were measured by CV in anhydrous DMF. The obtained potentials are compiled in Table 3. Typical cyclic voltammograms of all **DPHs** are shown in Figure S6 (SI). Moreover, the standard free energy changes of the electron transfer reaction  $\Delta G_{ET}$  of a **DPH** quencher with **Rh123** in its  $S_1$ ,  $T_1$ , or radical cation state  $R^{+\cdot}$  are given to check its energetic feasibility. The reaction with  $R^{+\cdot}$  also has to be considered, because it can be formed by two-step photolysis at very high irradiances.<sup>15</sup> The species-specific  $\Delta G_{ET}$  values were calculated by the Rehm–Weller eq 1 using the redox potentials and the excited state energies of the involved states of **Rh123**.<sup>31</sup>

Even though most redox reactions are electrochemically irreversible, the good linear correlation of the peak potentials with the Hammett  $\sigma$  coefficients<sup>72</sup> for the substituents of the aromatic **DPH** ring system support the interpretation that these potentials indeed reflect one-electron oxidation and reduction properties (Figure 4). Both the oxidation and the reduction potentials are reduced by electron donating groups (**Me<sub>2</sub>N-DPH**) and increased by electron withdrawing groups (**CF<sub>3</sub>-DPH**, **CN-DPH**, **bis-CF<sub>3</sub>-DPH**). The dotted line in Figure 4 indicates the substituent-specific feasibility for a triplet state reduction of **Rh123**. Quenchers with oxidation potentials that drop below this limit are able to quench the triplet state of **Rh123** by electron transfer.

All oxidizing processes of the excited states  $S_1$ ,  $T_1$ , and the photo-oxidized state  $R^{+\cdot}$  of **Rh123** are estimated to be endergonic ( $\Delta G_{ET} > 0$ ). Therefore, only the free energies of the reduction reactions of those states are given in Table 3. By

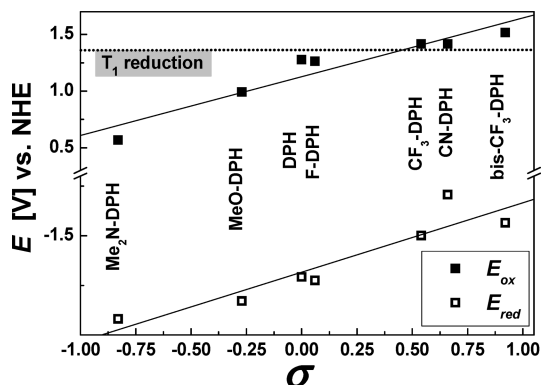


**Figure 4.** Oxidation and reduction potentials measured in DMF were plotted versus the Hammett coefficients. The linear relationship between the potentials and the Hammett coefficients is given by  $E_{\text{ox}} = 1.13 + 0.52 \times \sigma$  and  $E_{\text{red}} = -1.68 + 0.35 \times \sigma$ . The dotted line indicates the feasibility of the triplet state reduction of **Rh123**. Quenchers with oxidation potentials that drop below this limit are able to quench the triplet state of **Rh123** by electron transfer. In order to complete the Hammett plot on the side of the electron donating groups an additional methoxy-substituted **DPH** (**MeO-DPH**) ( $E_{\text{ox}} = 0.99$  V vs NHE,  $E_{\text{red}} = -1.83$  V) with a  $\sigma$  value of  $-0.27$  was measured. For further details, see SI.

introducing more electron withdrawing groups the quenching of the reduction reactions becomes less favorable. In order to avoid reduction of the  $S_1$  state of **Rh123** completely, even more electron deficient **DPHs** would be necessary. The  $T_1$  state of **Rh123** is expected to be also quenched effectively by electron transfer especially by **Me<sub>2</sub>N-DPH** (dotted line for  $\Delta G_{\text{ET}} = 0$  in Figure 4), whereas **bis-CF<sub>3</sub>-DPH** should not quench via electron transfer but still via TEET (for more discussions, see section 4.3).

**4.3. Fluorescence Correlation Spectroscopy Measures Triplet Quenching.** As the solubility of **DPHs** in water is very low, we studied them in ethanol. Because of the high solubility of the triplet quencher oxygen in ethanol, the rate constant for triplet relaxation  $k_T$  of **Rh123** is large, which results in a very low stationary triplet population in air-saturated solution. Therefore we bubbled the sample solution with a premixed  $O_2-N_2$  gas mixture, so that the oxygen concentration is reduced from 20% (air) to approximately 0.1%. To determine triplet parameters by FCS using eqs 2–4, a series of correlation curves at different mean irradiances  $I_0/2$  was measured.

**DPH.** Varying the irradiance, a typical set of correlation curves is displayed in Figure 5A for **Rh123** in the presence of the quencher **DPH** at a concentration of  $15.3 \mu\text{M}$ .

The analysis of correlation curves by eq 2 shows by equally distributed residuals that a diffusion term with the time  $t_d$  and a single triplet bunching term with the relaxation time  $t_T$  are sufficient to describe the data at low and medium irradiances. **DPH** is indeed a triplet quencher of **Rh123**, because the triplet amplitude  $T_{\text{eq}}$  (Figure 5C) and triplet time  $t_T$  decrease with increasing **DPH** concentration (Figure 5D). Global analysis of  $T_{\text{eq}}$  and  $t_T$  by eq 3 and 4 allowed us to compute  $k_{\text{ISC}}$  and  $k_T'$  for different **DPH** concentrations. Figure 5E shows that  $k_T'$  depends linearly on the **DPH** concentration as expected by eq 5, whereas  $k_{\text{ISC}}$  is independent of the quencher concentration  $[Q]$ . The determination of the slope yields a triplet quenching constant  $k_{\text{qT}}$  of **DPH** =  $4.9 \times 10^9 \text{ M}^{-1} \text{ s}^{-1}$ , which is close to the diffusion controlled value  $k_{\text{diff}} = 5.4 \times 10^9 \text{ M}^{-1} \text{ s}^{-1}$ .<sup>66</sup> It is important to note that  $k_{\text{ISC}}(0.1\% O_2) = 2 \times 10^5 \text{ s}^{-1}$  is 4.5 times smaller than  $k_{\text{ISC}}(\text{air})$ . In agreement with previous findings,<sup>14,73–75</sup> this indicates that, for **Rh123** oxygen enhanced ISC, there is also

an important fluorescence quenching pathway that leads to the formation of reactive singlet oxygen.

To discuss the distinct quenching effects on the  $T_1$  and  $S_1$  state, it is useful to define a quantum yield for quenching of the individual state  $X$  by  $\Phi_{\text{qX}} = (k_{\text{qX}} [Q]) / (k_X + k_{\text{qX}} [Q])$ . Here  $k_X$  is the inherent rate constant for the state deactivation, and  $k_{\text{qX}}$  is the bimolecular quenching constant. Considering a quencher with diffusion controlled  $k_{\text{diff}}$  at a concentration  $[Q] = 10 \mu\text{M}$  and the distinct  $S_1$  and  $T_1$  lifetimes of **Rh123** with  $1/k_0 = 4 \text{ ns}$  and  $1/k_T = 40 \mu\text{s}$ , the quantum yield of singlet quenching  $\Phi_{\text{qS}} = 0.02\%$  is more than 3000 times smaller than the quantum yield of triplet quenching  $\Phi_{\text{qT}} = 68\%$ . This selective quenching effect for **DPH** leads to a concomitant increase of the fluorescence count rate per molecule  $F_{\text{cpm}}$  (more than three times) and decrease of  $T_{\text{eq}}$  with increasing **DPH** concentration (Figure 5B and filled squares in Figure 6).

**Other DPHs.** In the following, we tested several substituted **DPHs** by FCS (**CF<sub>3</sub>-DPH** Figure S7, **F-DPH** Figure S8, **bis-CF<sub>3</sub>-DPH** Figure S9). The obtained triplet quenching constants  $k_{\text{qT}}$  are also listed in Table 3. Even if the limited accuracy (systematic error) may give errors of up to 5% and the precision (shot noise) is on average  $\pm 0.3 \times 10^9 \text{ M}^{-1} \text{ s}^{-1}$ , the difference of the quenching constants (approximately a factor of 2) is still significant and shows a systematic trend: The quenching constant decreases with increasing size or electronegativity of the **DPHs**. Moreover, considering size effects, the Smoluchowski equation predicts the opposite effect: the bimolecular quenching constant should rise and not decrease with increasing radius of the quencher; i.e., for the molecular dimensions of **Rh123** and the different **DPHs** (maximal radius increase 16%) an increase of  $k_{\text{qT}}$  of maximal 4.4% could be expected.

Another important aspect for applications as photoprotective agents is the solubility of triplet quenchers. In the case of **bis-CF<sub>3</sub>-DPH**, we observe a saturation of the beneficial effect above  $10 \mu\text{M}$ . Carotenoids and carotene derivatives are known to form complex aggregates in polar solvents already at low concentrations.<sup>76</sup> Therefore, in further studies, substituents should be used that improve the solubility of the **DPHs** in polar solvents or water.

**Effects of the Electron-Rich DPH: Me<sub>2</sub>N-DPH.** Figure 7A shows the FCS curves for **Rh123** in ethanol at a quencher concentration of  $8 \mu\text{M}$  **Me<sub>2</sub>N-DPH**. The correlation curves  $G(t_c)$  of **Rh123** measured in the presence of the quencher could not be described by eq 2 with a single bunching term. An additional bunching term is needed at a relaxation time of  $t_R = 77 \mu\text{s}$  with an amplitude  $R_{\text{eq}} = 0.30$ . Even though the decreased triplet amplitude  $T_{\text{eq}}$  indicates efficient triplet quenching (Figure 7B, upper panel,  $k_{\text{qT}} = 6 \pm 1 \times 10^9 \text{ M}^{-1} \text{ s}^{-1}$ ), surprisingly a decrease in fluorescence signal  $F_{\text{cpm}}$  is observed (Figure 7B, lower panel). Considering the possible electron transfer pathways in Table 3, one expects the formation of **Rh123** free radical anions  $R^{\cdot-}$  resulting from the reduction of the triplet state of the fluorophore by **Me<sub>2</sub>N-DPH**. As the oxygen concentration is low, this process produces another relatively long-lived dark state and competes with the beneficial effect of triplet quenching.

Next we changed the electron-donating dimethylamino groups in **Me<sub>2</sub>N-DPH** to electron-withdrawing quaternary ammonium groups to decrease the electron density of the quencher and thus to counteract its ability to reduce the  $T_1$  state of **Rh123**. At the same time, the solubility should be significantly increased. Using the Hammett  $\sigma$ -coefficient for  $\text{NH}_3^+$  ( $\sigma = 0.86$ ) and the relation of Figure 4, we are able to estimate  $E_{\text{ox}} = 1.58$  V vs NHE,

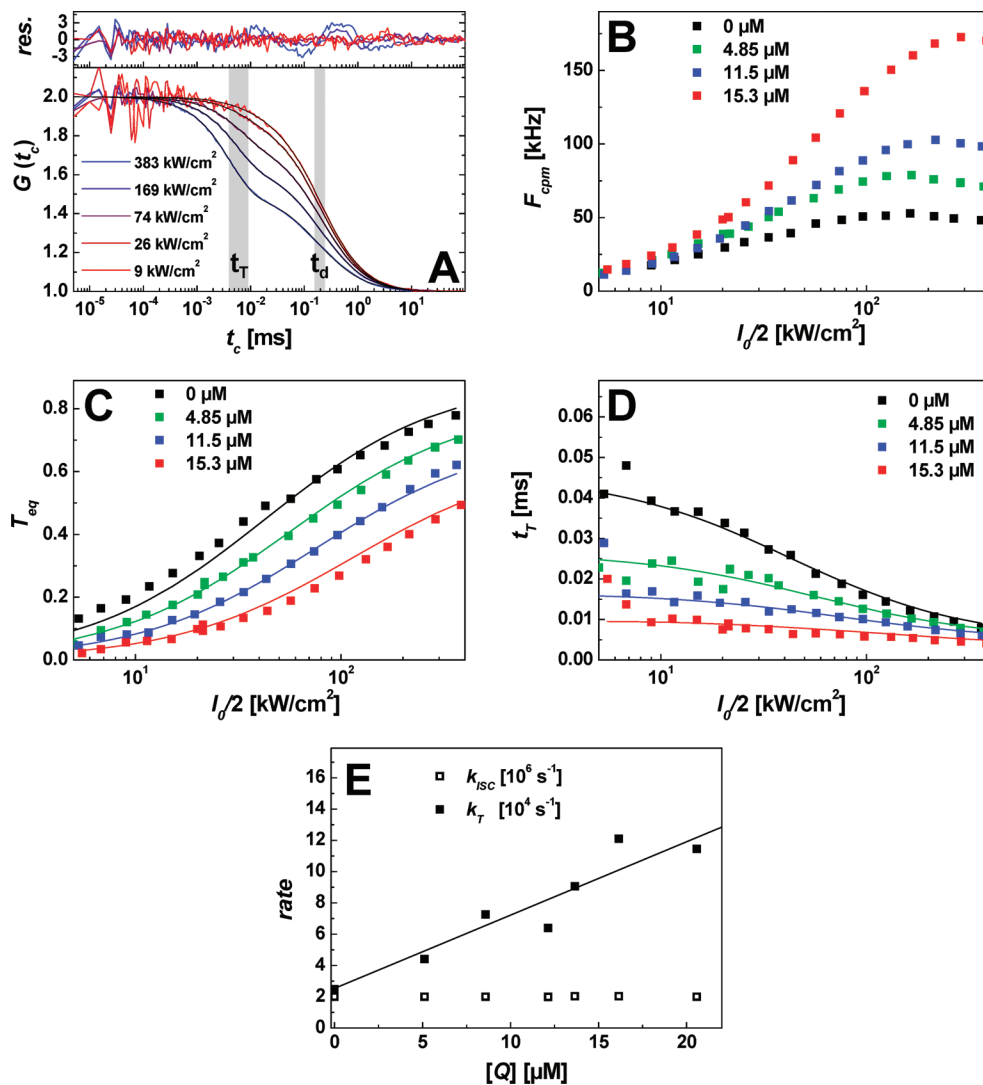


**Figure 5.** (A) Normalized correlation curves of **Rh123** in ethanol ( $[O_2] \sim 0.1\%$ ) with a quencher concentration of  $[Q] = 15.3 \mu\text{M}$  at different laser irradiances  $I_0/2$ . (B) Count rate per molecule  $F_{\text{cpm}}$ . (C,D) The parameters of the average molecule fraction in the triplet state  $T_{\text{eq}}$  and the triplet correlation time  $t_T$  according to eq 2 at 0, 4.85, 11.5, and 15.3  $\mu\text{M}$  **DPH** were plotted against the applied laser irradiance. The triplet parameters were fitted globally to eqs 3 and 4 to give  $k_{\text{ISC}}$  and  $k_T'$  for each concentration. (E) The slope of the observed triplet relaxation rates  $k_T'$  with the concentration is equal to the triplet quenching rate  $k_{\text{QT}} = 4.9 \times 10^9 \text{ M}^{-1} \text{ s}^{-1}$ .

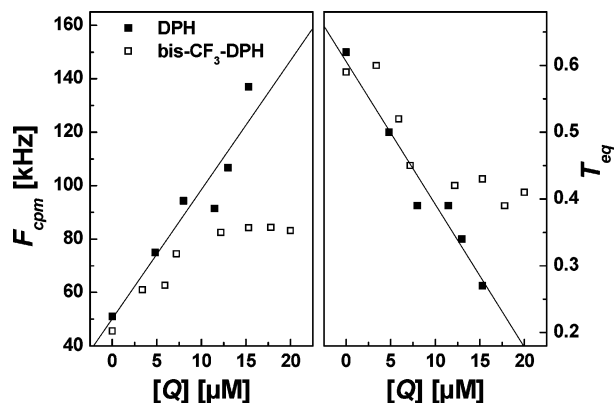


**Figure 6.** Dependence of the fluorescence signal  $F_{\text{cpm}}$  and the triplet population  $T_{\text{eq}}$  of **Rh123** on the concentration of **DPH** (■) and **bis-CF<sub>3</sub>-DPH** (□) at a laser irradiance of  $I_0/2 = 100 \text{ kW/cm}^2$ .

which is similar to the potential of **bis-CF<sub>3</sub>-DPH** (see Table 3). Thus, no triplet quenching by electron transfer should be possible.

Two derivatives of **DPH** with quaternary ammonium groups have been studied (see Section 1, SI): (I) **Me<sub>2</sub>N-DPH** was dissolved in ethanol containing 1% sulfuric acid to give **HMe<sub>2</sub>N<sup>+</sup>-DPH** (*all-E*)-1,6-bis-[4-(dimethylammonium)phenyl]hexa-1,3,5-triene bis hydrogen sulfate (Figure S2, the acidic conditions do not affect the cationic dye **Rh123**). (II) An alkylated **DPH** with a quaternary ammonium group was synthesized (*all-E*)-1,6-bis-[4-(ethyltrimethylammonium)phenyl]hexa-1,3,5-triene bis *p*-toluenesulfonate **EtMe<sub>2</sub>N<sup>+</sup>-DPH** (Figure S3). It is noteworthy to mention that the specific spectral red shift in absorption of **Me<sub>2</sub>N-DPH** vanishes completely upon quaternization of the amino groups (see Figures S2 and S3). The resulting UV/vis absorption spectra are now identical to the other **DPHs**. Considering **HMe<sub>2</sub>N<sup>+</sup>-DPH**, the computed vertical  $T_1$  energy for absorption  $E_T(^3Q_1 \leftarrow ^1Q_0) = 1.75 \text{ eV}$  does not deviate from the other **DPHs** (see section 4.1), so that TEET should be possible. Surprisingly, FCS experiments with **HMe<sub>2</sub>N<sup>+</sup>-DPH** and **EtMe<sub>2</sub>N<sup>+</sup>-DPH** showed no changes in signal strength or triplet population of **Rh123**. No differences were found in the FCS curves of **Rh123** measured in ethanol or ethanol with sulfuric acid as control. The count rate per molecule as well as the triplet amplitude and the diffusion time remained unchanged.

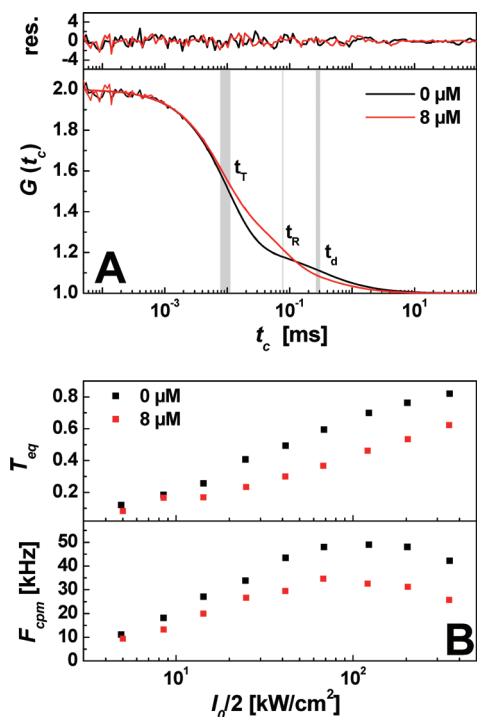


**Figure 7.** (A) Normalized correlation curves of **Rh123** in ethanol at  $I_0/2 = 200 \text{ kW/cm}^2$ . In the presence of  $8 \mu\text{M Me}_2\text{N-DPH}$ , an additional bunching term is needed to describe the curve. The fitted relaxation parameters were  $T_{\text{eq}} = 0.76$  and  $t_T = 11 \mu\text{s}$  for **Rh123** and  $T_{\text{eq}} = 0.53$ ,  $t_T = 7.7 \mu\text{s}$ ,  $R_{\text{eq}} = 0.30$  and  $t_R = 77 \mu\text{s}$  for **Me<sub>2</sub>N-DPH**. (B) Average fraction of molecules in the triplet state  $T_{\text{eq}}$  and fluorescence count rate per molecule  $F_{\text{cpm}}$  as a function of the applied laser irradiance.

It seems reasonable that the positive charges of the two **RMe<sub>2</sub>N<sup>+</sup>-DPH** derivatives are responsible for the lack of activity (see Conclusions).

## 5. Conclusions

**DPHs** quench the triplet state of **Rh123** effectively with specific quenching rates varying by more than a factor of 2 from nearly diffusion-controlled ( $4.9 \times 10^9 \text{ M}^{-1} \text{ s}^{-1}$ ) to lower values. Possible reasons for the observed differences raise the question of the detailed mechanism. The best quenching effect is obtained with the parent compound **DPH**, whereas the quenching efficiency is reduced with larger substituents and increasing oxidation potentials. Two channels for triplet state deactivation by the **DPHs** can be discussed.<sup>77,78</sup> First, looking at the energetic levels from the quantum mechanical calculations, the free energy for Dexter TEET from the fluorescent dye to the **DPHs**  $\Delta G_{\text{TEET}}$  should be exergonic ( $\Delta G_{\text{TEET}} < -0.2 \text{ eV}$ , see section 4.1 and Table 1). Beyond that, triplet quenching by an additional electron transfer pathway<sup>17</sup> is considered to be feasible for those **DPHs**, where the free energy  $\Delta G_{\text{ET}}(T_1)$  is exergonic (see Table 3). In case of **Me<sub>2</sub>N-DPH** ( $\Delta G_{\text{ET}}(T_1) = -0.77 \text{ eV}$ ), a significant population of a newly long-lived dark state is detected by FCS, which could be assigned to free radicals. **DPH** and **F-DPH** differ in  $k_{\text{qT}}$ , but they have approximately the same  $\Delta G_{\text{TEET}}$  and  $\Delta G_{\text{ET}}(T_1)$ . Thus additional effects by substituents, which are important for the Dexter ET by influencing the spectral overlap, must be considered as well: (I) Altering steric hindrance,<sup>79,80</sup> (II) change in electron density in the relevant orbitals and orbital overlap,<sup>81</sup> or (III) introduction of intermolecular Coulombic attraction or repulsion.

For example, larger steric hindrance by the **CF<sub>3</sub>** groups might contribute to the reduced quenching efficiency of **CF<sub>3</sub>-DPH** and

**bis-CF<sub>3</sub>-DPH**. Moreover, the Coulomb repulsion between the two positively charged molecules **RMe<sub>2</sub>N<sup>+</sup>-DPH** and **Rh123** increases their interaction distance, which explains the complete loss of the ability for triplet quenching. To conclude, the ability of **DPH** derivatives to quench dye triplet states is governed by a delicate interplay of steric, Coulombic and electronic effects. Electron deficient **DPHs** have indeed beneficial effects on the fluorescence rate of **Rh123** by reducing the triplet state population and by avoiding the formation of other long-lived dark states.

**Acknowledgment.** The present work has been performed as a project of the SFB 663 (A8, C1) at the Heinrich-Heine-Universität Düsseldorf. We thank Jerker Widengren and Ralf Kühnemuth for very helpful discussions on FCS. This work is dedicated to the memory of Prof. Dr. Hans-Dieter Martin, who passed away on March 8, 2009.

**Supporting Information Available:** Section 1 contains a detailed description of the synthesis and characterization for the different **DPHs**. In Section 2, further information on excited state relaxation of the **DPHs** (2.1), the absorption (2.2), and the emission spectra (2.3) of the **DPHs** as well as the multi Gaussian analysis of these (2.2 and 2.3) are given. Furthermore, Section 2 gives the cyclic voltammograms for the **DPHs** (2.4) and the FCS data for the **DPHs** not shown in the main manuscript (2.5). This material is available free of charge via the Internet at <http://pubs.acs.org>.

## References and Notes

- (1) Yamashita, M.; Kuniyasu, A.; Kashiwagi, H. *J. Chem. Phys.* **1977**, *66*, 986.
- (2) Drexhage, K. H.; Schäfer, F. P. Structure and properties of laser dyes. In *Topics in Applied Physics*; Springer Verlag: Berlin, 1973; Vol. 1, pp 144.
- (3) Gonçalves, M. S. T. *Chem. Rev.* **2009**, *109*, 190.
- (4) Pawley, J. B. *Handbook of Biological Confocal Microscopy*, 3rd ed.; Springer: New York, 2006.
- (5) Hell, S. W. *Science* **2007**, *316*, 1153.
- (6) Widengren, J.; Kudryavtsev, V.; Antonik, M.; Berger, S.; Gerken, M.; Seidel, C. A. M. *Anal. Chem.* **2006**, *78*, 2039.
- (7) Hausteiner, E.; Schwille, P. *Annu. Rev. Biophys. Biomol. Struct.* **2007**, *36*, 151.
- (8) Widengren, J.; Chmyrov, A.; Eggeling, C.; Löfdahl, P. A.; Seidel, C. A. M. *J. Phys. Chem. A* **2007**, *111*, 429.
- (9) Vogelsang, J.; Cordes, T.; Forthmann, C.; Steinhauer, C.; Tinnefeld, P. *Proc. Natl. Acad. Sci. U.S.A.* **2009**, *106*, 8107.
- (10) Hofkens, J.; Cotlet, M.; Vosch, T.; Tinnefeld, P.; Weston, K. D.; Ego, C.; Grimdale, A.; Müllen, K.; Beljonne, D.; Bredas, J. L.; Jordens, S.; Schweitzer, G.; Sauer, M.; De Schryver, F. *Proc. Natl. Acad. Sci. U.S.A.* **2003**, *100*, 13146.
- (11) Liphardt, B.; Lüttke, W. *Opt. Commun.* **1983**, *48*, 129.
- (12) Sauer, M.; Han, K. T.; Müller, R.; Schulz, A.; Tadday, R.; Seeger, S.; Wolfrum, J.; Arden-Jacob, J.; Deltau, G.; Marx, N. J.; Drexhage, K. H. *J. Fluoresc.* **1993**, *3*, 131.
- (13) Ernsting, N. P.; Kaschke, M.; Kleinschmidt, J.; Drexhage, K. H.; Huth, V. *Chem. Phys.* **1988**, *122*, 431.
- (14) Eggeling, C.; Widengren, J.; Rigler, R.; Seidel, C. A. M. Photostabilities of fluorescent dyes for single-molecule spectroscopy: Mechanisms and experimental methods for estimating photobleaching in aqueous solution. In *Applied Fluorescence in Chemistry, Biology and Medicine*; Springer: Berlin, 1999; pp 193.
- (15) Eggeling, C.; Widengren, J.; Rigler, R.; Seidel, C. A. M. *Anal. Chem.* **1998**, *70*, 2651.
- (16) Widengren, J.; Rigler, R. *Bioimaging* **1996**, *4*, 149.
- (17) Vogelsang, J.; Kasper, R.; Steinhauer, C.; Person, B.; Heilemann, M.; Sauer, M.; Tinnefeld, P. *Angew. Chem., Int. Ed.* **2008**, *47*, 5465.
- (18) Rasnik, I.; McKinney, S. A.; Ha, T. *Nat. Methods* **2006**, *3*, 891.
- (19) Ferguson, M. W.; Beaumont, P. C.; Jones, S. E.; Navaratnam, S.; Parsons, B. *J. Phys. Chem. Chem. Phys.* **1999**, *1*, 261.
- (20) Ringemann, C.; Schönle, A.; Giske, A.; von Middendorff, C.; Hell, S. W.; Eggeling, C. *ChemPhysChem* **2008**, *9*, 612.
- (21) Förster, T. *Discussions Faraday Soc.* **1959**, *7*.
- (22) Förster, T. *Ann. Phys.* **1948**, *2*, 55.

- (23) Förster, T. *Fluoreszenz Organischer Verbindungen*; Vandenhoeck and Ruprecht: Göttingen, Germany, 1951.
- (24) Dexter, D. L. *J. Chem. Phys.* **1953**, *21*, 836.
- (25) Rehm, D.; Weller, A. *Israel J. Chem.* **1970**, *8*, 259.
- (26) Rehm, D.; Weller, A. *Z. Phys. Chem.* **1970**, *69*, 183.
- (27) Marcus, R. A. *J. Chem. Phys.* **1956**, *24*, 966.
- (28) Kavarnos, G. J.; Turro, N. J. *Chem. Rev.* **1986**, *86*, 401.
- (29) In order to describe the transitions involved in these processes we followed IUPAC conventions and denoted the excited state first and the ground state last. Thus absorption is marked by “←” and an emission is marked by “→”.
- (30) Mills, I.; Cvitas, T.; Homann, K.; Kallay, K.; Kuchitsu, K. *Quantities, Units and Symbols in Physical Chemistry*, 2nd ed.; Blackwell Science: Oxford, U.K., 1993.
- (31) Wardman, P. J. *Phys. Chem. Ref. Data* **1989**, *18*, 1637.
- (32) Polívka, T.; Sundström, V. *Chem. Rev.* **2004**, *104*, 2021.
- (33) Furuichi, K.; Sashima, T.; Koyama, Y. *Chem. Phys. Lett.* **2002**, *356*, 547.
- (34) Hilinski, E. F.; McGowan, W. M.; Sears, D. F.; Saltiel, J. J. *Phys. Chem.* **1996**, *100*, 3308.
- (35) Ye, J. F.; Chen, H.; Note, R.; Mizuseki, H.; Kawazoe, Y. *Int. J. Quantum Chem.* **2007**, *107*, 2006.
- (36) For the calculations regarding RH123, the ethyl ester was used instead of the methyl ester.
- (37) Sonoda, Y.; Kawanishi, Y.; Ikeda, T.; Goto, M.; Hayashi, S.; Yoshida, Y.; Tanigaki, N.; Yaso, K. *J. Phys. Chem. B* **2003**, *107*, 3376.
- (38) Zhuang, Z. P.; Kung, M. P.; Kung, H. F. *J. Med. Chem.* **2006**, *49*, 2841.
- (39) Trepanier, V. E.; Fillion, E. *Organometallics* **2007**, *26*, 30.
- (40) Kauffman, J. M.; Moyna, G. *J. Org. Chem.* **2003**, *68*, 839.
- (41) Alford, P. C.; Palmer, T. F. *Chem. Phys. Lett.* **1982**, *86*, 248.
- (42) Alford, P. C.; Palmer, T. F. *Chem. Phys. Lett.* **1986**, *127*, 19.
- (43) Sonoda, Y.; Kwok, W. M.; Petrusek, Z.; Ostler, R.; Matousek, P.; Towrie, M.; Parker, A. W.; Phillips, D. *J. Chem. Soc. Perkin Trans. 2* **2001**, 308.
- (44) Sonoda, Y.; Morii, H.; Sakuragi, M.; Suzuki, Y. *Chem. Lett.* **1998**, 349.
- (45) Barluenga, J.; Moriel, P.; Aznar, F.; Valdes, C. *Adv. Synth. Catal.* **2006**, *348*, 347.
- (46) Schäfer, A.; Huber, C.; Ahlrichs, R. *J. Chem. Phys.* **1994**, *100*, 5829.
- (47) Kohn, W.; Sham, L. J. *Phys. Rev.* **1965**, *140*, A1133.
- (48) Becke, A. D. *J. Chem. Phys.* **1993**, *98*, 5648.
- (49) Lee, C. T.; Yang, W. T.; Parr, R. G. *Phys. Rev. B* **1988**, *37*, 785.
- (50) Furche, F.; Ahlrichs, R. *J. Chem. Phys.* **2002**, *117*, 7433.
- (51) Ahlrichs, R.; Bär, M.; Häser, M.; Horn, H.; Kolmel, C. *Chem. Phys. Lett.* **1989**, *162*, 165.
- (52) Schade, B.; Hagen, V.; Schmidt, R.; Herbrich, R.; Krause, E.; Eckardt, T.; Bendig, J. *J. Org. Chem.* **1999**, *64*, 9109.
- (53) Klamt, A.; Schüürmann, G. *J. Chem. Soc., Perkin Trans. 2* **1993**, 799.
- (54) Grimme, S.; Waletzke, M. *J. Chem. Phys.* **1999**, *111*, 5645.
- (55) Marian, C. M.; Gilka, N. *J. Chem. Theory Comput.* **2008**, *4*, 1501.
- (56) Kleinschmidt, M.; Marian, C. M.; Waletzke, M.; Grimme, S. *J. Chem. Phys.* **2009**, *130*, 044708.
- (57) Magde, D.; Elson, E. L.; Webb, W. W. *Biopolymers* **1974**, *13*, 29.
- (58) Elson, E. L.; Magde, D. *Biopolymers* **1974**, *13*, 1.
- (59) Magde, D.; Elson, E. L.; Webb, W. W. *Phys. Rev. Lett.* **1972**, *29*, 705.
- (60) Widengren, J.; Mets, Ü.; Rigler, R. *J. Phys. Chem.* **1995**, *99*, 13368.
- (61) Enderlein, J.; Gregor, I.; Patra, D.; Dertinger, T.; Kaupp, U. B. *ChemPhysChem* **2005**, *6*, 2324.
- (62) Eggeling, C.; Volkmer, A.; Seidel, C. A. M. *ChemPhysChem* **2005**, *6*, 791.
- (63) Christensen, R. L.; Barney, E. A.; Broene, R. D.; Galinato, M. G. I.; Frank, H. A. *Arch. Biochem. Biophys.* **2004**, *430*, 30.
- (64) Dupuy, B.; Montagu, M. *Analyst* **1997**, *122*, 783.
- (65) Kohler, B. E.; Itoh, T. *J. Phys. Chem.* **1988**, *92*, 5120.
- (66) Murov, S. L.; Carmichael, I.; Hug, G. L. *Handbook of Photochemistry*; Marcel Dekker Inc.: New York, 1993.
- (67) Saltiel, J.; Crowder, J. M.; Wang, S. J. *J. Am. Chem. Soc.* **1999**, *121*, 895.
- (68) Evans, D. F.; Tucker, J. N. *J. Chem. Soc., Faraday Trans. 2* **1972**, *68*, 174.
- (69) Heupel, M.; Gregor, I.; Becker, S.; Thiel, E. *Int. J. Photoenergy* **1999**, *1*, 165.
- (70) Menzel, R.; Bornemann, R.; Thiel, E. *Phys. Chem. Chem. Phys.* **1999**, *1*, 2435.
- (71) Kunavin, N. I.; Nurmukhametov, R. N.; Khachaturova, G. T. *Zh. Prikl. Spektrosk.* **1977**, *26*, 1023.
- (72) Hansch, C.; Leo, A.; Taft, R. W. *Chem. Rev.* **1991**, *91*, 165.
- (73) Gregor, I.; Heupel, M.; Thiel, E. *Chem. Phys.* **2001**, *272*, 185.
- (74) Stracke, F.; Heupel, M.; Thiel, E. *J. Photochem. Photobiol. A* **1999**, *126*, 51.
- (75) Schweitzer, C.; Schmidt, R. *Chem. Rev.* **2003**, *103*, 1685.
- (76) Köpsel, C.; Moltgen, H.; Schuch, H.; Auweter, H.; Kleinermanns, K.; Martin, H. D.; Bettermann, H. *J. Mol. Struct.* **2005**, *750*, 109.
- (77) Balzani, V.; Bolletta, F.; Scandola, F. *J. Am. Chem. Soc.* **1980**, *102*, 2152.
- (78) Nau, W. M.; Scaiano, J. C. *J. Phys. Chem.* **1996**, *100*, 11360.
- (79) Wamser, C. C.; Medary, R. T.; Kochevar, I. E.; Turro, N. J.; Chang, P. L. *J. Am. Chem. Soc.* **1975**, *97*, 4864.
- (80) Cheng, G.; Peng, X.; Hao, G.; Kennedy, V. O.; Ivanov, I. N.; Knappenberger, K.; Hill, T. J.; Rodgers, M. A. J.; Kenney, M. E. *J. Phys. Chem. A* **2003**, *107*, 3503.
- (81) Albinsson, B.; Mårtensson, J. *J. Photochem. Photobiol. C* **2008**, *9*, 138.

JP909033X